EURAMET
European Association of National Metrology Institutes

Open Access Repository eprint

Terms and Conditions: Users may access, download, store, search and print a hard copy of the article. Copying must be limited to making a single printed copy or electronic copies of a reasonable number of individual articles or abstracts. Access is granted for internal research, testing or training purposes or for personal use in accordance with these terms and conditions. Printing for a for-fee-service purpose is prohibited.

Title: Counting the atoms in a 28Si crystal for a new kilogram definition
Author(s): Andreas, B.; Azuma, Y.; Bartl, G.; Becker, P.; Bettin, H.; Borys, M.; Busch, I.; Fuchs, P.; Fujii, K.; Fujimoto, H.; Kessler, E.; Krumrey, M.; Kuetgens, U.; Mizushima, N.; Nicolaus, A.; Picard, A.; Pramann, A.; Rienitz, O.; Schiel, D.; Valkiers, S.; Waseda, A.; Zakel, S.
Journal: Metrologia
Year: 2011, Volume: 48, Issue: 2
DOI: doi:10.1088/0026-1394/48/2/S01

Funding programme: iMERA-Plus: Call 2007 SI and Fundamental Metrology
Project title: T1.J1.1: e-Mass: The watt balance route towards a new definition of the kilogram

Copyright note: This is an author-created, un-copyedited version of an article accepted for publication in Metrologia. IOP Publishing Ltd is not responsible for any errors or omissions in this version of the manuscript or any version derived from it. The definitive publisher-authenticated version is available online at doi:10.1088/0026-1394/48/2/S01

EURAMET
Secretariat
Bundesallee 100
38116 Braunschweig, Germany

Phone: +49 531 592-1960
Fax: +49 531 592-1969
secretariat@euramet.org
www.euramet.org

Counting the atoms in a ^{28}Si crystal for a new kilogram definition

B Andreas[1], Y Azuma[2], G Bartl[1], P Becker[1*)], H Bettin[1], M Borys[1], I Busch[1], P Fuchs[3], K Fujii[2], H Fujimoto[2], E Kessler[4], M Krumrey[1], U Kuetgens[1], N Kuramoto[2], G Mana[5], E Massa[5], S Mizushima[2], A Nicolaus[1], A Picard[6], A Pramann[1], O Rienitz[1], D Schiel[1], S Valkiers[7], A Waseda[2] and S Zakel[1]

[1]Physikalisch-Technische Bundesanstalt PTB, Bundesallee 100, 38116 Braunschweig, Germany
[2]National Metrology Institute of Japan NMIJ, 1-1-1 Umezono, Tsukuba, Ibaraki 305-8563, Japan
[3]Bundesamt für Metrologie METAS, Lindenweg 50, 3003 Bern-Wabern, Switzerland
[4]National Institute of Standards and Technology NIST, 100 Bureau Drive, Gaithersburg, MD 20899, USA
[5]Istituto Nazionale di Ricerca Metrologica INRIM, str. delle cacce 91, 10135 Torino, Italy
[6]Bureau International des Poids et Mesures BIPM, Pavillon de Breteuil, 92312 Sèvres Cedex, France
[7]Institute for Reference Materials and Measurements IRMM, Retieseweg 111, B-2440 Geel, Belgium

*) corresponding author, peter.becker@ptb.de

Abstract

This paper concerns an international research project aimed at determining the Avogadro constant by counting the atoms in an isotopically enriched silicon crystal. The counting procedure was based on the measurement of the molar volume and the volume of an atom in two 1 kg crystal-spheres. The novelty was the use of isotope dilution mass spectrometry as a new and very accurate method for the determination of the molar mass of enriched silicon. Because of an unexpected metallic contamination of the sphere surfaces, the relative measurement uncertainty, 3×10^{-8} N_A, results larger by a factor 1.5 than that targeted. The measured value of the Avogadro constant, N_A = 6.022 140 82 (18) $\times 10^{23}$ mol^{-1} is the most accurate input datum for the kilogram redefinition and differs by 16×10^{-8} N_A from the CODATA 2006 adjusted value. This value is midway between the NIST and NPL watt-balance values.

PACS numbers: 06.20.-f; 06.20.Jr; 61.05.C-; 81.10.Fq; 42.87.g

1. Introduction

The extent and accuracy to which our theoretical models and measurement techniques are valid across the different sectors of physics is a subject of utmost interest. Accurate measurements of fundamental constants of physics are a way of carrying out such investigations and of testing the limits of our knowledge and technologies. In tests of this kind, the measurement of the Avogadro constant, N_A, holds a prominent position and it is both input and output of the least squares adjustment of the fundamental constants, because it connects microphysics and macrophysics.

N_A is the number of atoms or molecules in a mole of a pure substance, for instance, the number of atoms (unbound, at rest, and in their ground state) in 12 g of the carbon isotope ^{12}C. Therefore, N_A expresses the ^{12}C mass in kilogram according to $M(^{12}C) = N_A m(^{12}C)$, where $M(^{12}C) = 12$ g/mol and $m(^{12}C)$ are the molar mass and the mass of the ^{12}C atom, respectively. Many different N_A measurements, from that of Loschmidt to that of Perrin, supported the Maxwell and Boltzmann descriptions of matter in terms of atoms [1]. N_A establishes detailed balances in chemical reactions. It is a scale factor to convert atomic quantities and macroscopic quantities also as regards electromagnetism and thermodynamics, as it connects the electron charge e with a macroscopically measurable electrical charge via $F = N_A e$, where F is the Faraday constant; it also connects statistical mechanics with thermodynamics via $R = N_A k_B$, where R and k_B are the universal gas constant and the Boltzmann constant, respectively.

The Avogadro constant is an important input datum for the redefinition of the unit of mass, the kilogram, on the basis of a fundamental physical constant. The kilogram is the only base unit still defined by a material prototype as stated by the 1st General Conference on Weights and Measures in 1889. The mass of the international prototype expressed in terms of the SI unit is invariable by definition, but, since 1889 the mass differences between the international prototype and its national copies drifted by about 50 μg, or 5×10^{-8} in relative terms, on the average. Though a forthcoming new definition of the kilogram [2] will be based on the Planck constant, h, the value of h can be calculated from that of N_A without losing accuracy by using the molar Planck constant, $N_A h$. In fact, the $N_A h$ value is very well known via the measurement of the Rydberg constant, $R_\infty = \alpha^2 M(e^-)c/(2N_A h)$, where α is the fine structure constant, $M(e^-)$ the molar mass of the electron, and c the speed of light. The relative uncertainties of the Rydberg and the fine-structure constants and of the electron molar mass are 6.6×10^{-12}, 6.8×10^{-10}, and 4.2×10^{-10}, respectively, whereas the speed of light is an exact quantity. Therefore, an accurate measurement of N_A is of paramount importance because it also provides an accurate and independent determination of h.

Whereas the uncertainty of the mass of the international prototype is zero by convention, any *mise en pratique* of a new definition will fix an uncertainty to the international prototype. In order to ensure continuity to mass metrology, it has been agreed that the relative uncertainty of any new realization must not exceed 2×10^{-8}. At present, two different experiments have the potential to meet this challenge: One is the watt-balance experiment which was first proposed in 1975 by Kibble [3]. It aims at measuring the Planck constant by the virtual comparison of mechanical power with electrical power. The watt-balance result is a measurement of the $m(\mathfrak{K})/h$ ratio, where $m(\mathfrak{K})$ is the mass of the international prototype. The other experiment, the basic principles of which are described by Becker [1], was outlined by Zosi [4] in 1983 and requires atom counting in 1 kg quasi-perfect single-crystal silicon spheres. With this method, crystallization acts as a "low noise amplifier" making the lattice parameter accessible to macroscopic measurements, thus avoiding single atom counting. Silicon is used because it is one of the best known materials and, owing to the demands of the semiconductor industry it can be grown to high-purity, large and almost perfect single crystals.

Since 1998, a relative 1.2×10^{-6} discrepancy has been observed from comparison of the results of the watt-balance and Si crystal experiments [5]. Subsequently, it was conjectured that this discrepancy originated from the difficulty of accurately determining the isotopic composition of a natural silicon crystal, a key measurement for the N_A determination. To solve this problem, we started a research project to repeat the measurement by use of a silicon crystal highly enriched with the ^{28}Si isotope. In this way, the difficult absolute calibration of the mass spectrometer, having the required small uncertainty, could be overcome by applying isotope dilution mass spectrometry (IDMS) combined with multicollector inductively coupled plasma mass spectrometry.

The project started in 2004 with isotope enrichment. Subsequently, a polycrystal was grown by chemical vapour deposition and, in 2007, the 5 kg ^{28}Si boule shown in figure 1 was grown [6]. As an unexpected by-product, the availability of highly enriched and highly pure ^{28}Si single crystals, as well as of highly enriched ^{29}Si and ^{30}Si crys-

tals, brought about physical and technological investigations in the fields of quantum computing and semiconductor spectroscopy [7].

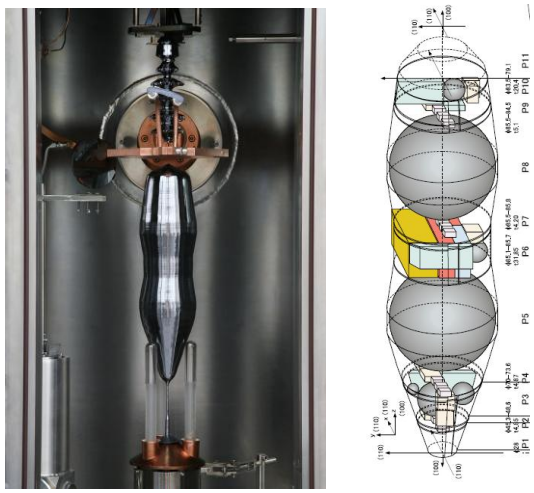

Figure 1. The float-zone ^{28}Si crystal and its cutting plan. To determine density, two spheres (AVO28-S5 and AVO28-S8) were manufactured from the two bulges. To determine the lattice parameter, an X-ray interferometer was cut from the material between the two spheres (yellow part of the cutting plan). The enrichment is higher than 0.99995.

2. Determination of the crystal quantities

The measurement of the Avogadro constant is based on

$$N_A = nM/(\rho a^3), \tag{1}$$

where $n = 8$ is the number of atoms per unit cell of a silicon crystal and ρ, M, and a are the density, molar mass, and lattice parameter, respectively. To implement the measurement equation (1) in practice, an isotopically enriched silicon crystal was grown and two ^{28}Si kilogram artefacts shaped as quasi-perfect spheres were manufactured; their mass and volume were accurately measured and their surfaces were chemically and physically characterized at the atomic scale. Unfortunately, the sphere surfaces were contaminated with metal silicides during polishing; this hampered progress and impaired the measurement accuracy.

In real crystals, the lattice spacing and density are affected by impurity atoms and vacancies, which change the atom distances according to the individual binding conditions. Equation (1) was applied to each sphere separately. Therefore, since the molar mass, lattice parameter, and volume used in (1) are those of each sphere, the sphere masses were corrected for the impurity atoms and vacancies. In this way, we calculated the mass of equivalent spheres, having the same volume and lattice parameter as the real ones, but having a Si atom in each lattice site.

The lattice parameter and the molar mass of the spheres were not measured directly, but in samples cut before and after them. All the samples cut from the ^{28}Si crystal, identified as 28Si-10Pr11, were labelled after a systematic identification system, named SIS code. The centres of AVO28-S5 and AVO28-S8 spheres were at a distance of 226 cm and 367 cm from the seed; the centre of the X-ray interferometer (XINT) was at a distance of 306 cm. To substantiate the necessary interpolations, the homogeneity of the molar mass, density, and lattice parameter, as well as the crystal structure, imperfections, and impurities, were investigated by different methods. Interpolations were carried out separately for both spheres; the consistency of the values obtained by the separate application of (1) is a further confirmation of the crystal homogeneity.

Temperature is a critical element; the density and the lattice parameter must be measured at the same temperature. This was achieved by controlling the thermal stability and thermal gradient of the spheres and X-ray interferometer, by periodic calibrations of the standard platinum resistance thermometers against the INRIM's and PTB's realizations of the 1990 temperature scale, and by demonstrating that the measurement chains used in the density, volume, and lattice parameter determinations are consistent to within 1 mK with a travelling 20 °C electronic reference point. The uncertainties of temperature measurements were: 1.0 mK (lattice parameter), 0.80 mK (PTB's volume measurement), and 0.62 mK (NMIJ's volume measurement).

The isotope enrichment was carried out by the Central Design Bureau of Machine Building in St. Petersburg by centrifugation of SiF_4 gas. After conversion of the enriched gas into SiH_4, a polycrystal was grown by chemical vapour deposition at the Institute of Chemistry of High-Purity Substances of the Russian Academy of Sciences in Nizhny Novgorod. The 5 kg crystal was grown and purified by multiple float-zone crystallizations at the Leibniz-Institut für Kristallzüchtung in Berlin. The concentrations of the residual impurities (carbon, oxygen, and boron) were determined at the PTB by optical spectroscopy. The concentration of the vacancy-related defects was deduced from positron lifetime spectroscopy at the Halle University. The results are given in section 2.1.

The amount-of-substance fractions of the Si isotopes were measured by the IRMM, via gas mass spectrometry of the SiF_4 gas, and by the PTB, via isotope dilution combined with multicollector inductively coupled plasma mass spectrometry. The isotope fractions were measured also at the Institute of Mineral Resources (IMR) of the Chinese Academy of Science via gas mass spectrometry, but with use of a different preparation of the SiF_4 gas based on fluorination by BrF_5 and at the Institute for Physics of Microstructures of the Russian Academy of Sciences by means of a secondary ion mass spectrometer using a time-of-flight mass analyzer. The results are given in section 2.2.

To measure the lattice parameter, the INRIM upgraded a combined X-ray and optical interferometer to expand the measurement capability to many centimetres and to achieve a relative uncertainty approaching 10^{-9}. To exploit this capability, the PTB manufactured an X-ray interferometer with an unusually 5 cm long analyzer crystal. To demonstrate the crystal homogeneity, the NIST measured the lattice parameter of crystal samples, taken above and below the two spheres; the measurements were comparisons against a natural Si crystal calibrated by X-ray interferometry. The NMIJ checked the crystal perfection by a strain topography carried out by means of a self-referenced X-ray diffractometer at the Photon Factory of the High Energy Accelerator Research Organization (KEK, Japan). Detailed results are given in section 2.3.

Sections from 2.4 to 2.7 describe the measurement of the ^{28}Si-sphere density. The spheres were shaped and optically polished by the Australian Centre for Precision Optics. Their volumes were determined via diameter measurements. The NMIJ measured several hundred diameters by means of an optical interferometer with a flat étalon. The PTB used a spherical Fizeau interferometer which allowed about 10^5 diameters to be measured and a complete topographical mapping to be obtained. The PTB, NMIJ, and METAS characterized the sphere surfaces as regards composition, mass, and thickness by X-ray fluorescence, near edge X-ray absorption fine structure spectroscopy, X-ray reflectometry, X-ray photoelectron spectroscopy, and optical spectral ellipsometry (section 2.4). Mass comparisons of the two spheres with Pt-Ir kilogram standards were carried out in vacuum by the BIPM, NMIJ, and PTB (section 2.6). Owing to air-vacuum transfer, a sorption correction, which was measured by means of sorption artefacts, had to be considered for the Pt-Ir standards. The sphere densities reported in section 2.7 were calculated from the mass to volume ratio, account being taken of the influence of the surface layer. In order to assess the crystal homogeneity and the measured values of the sphere densities, density comparison by hydrostatic and pressure-of-flotation methods were carried out by the NMIJ and PTB.

The final N_A values obtained from the two spheres are given in section 3 together with their uncertainty budget; in section 4, our final result is compared with those of the watt-balance experiments.

2.1. Point defects

The impurity concentrations N_i were measured by infrared spectroscopy [8] and are summarized in table 1. The crystal is not contaminated by nitrogen because it was not nitrogen doped during float-zone purification. The vacancy content was measured by means of positron lifetime spectroscopy, the result being $N_{vac} = 3.3(1.1) \times 10^{14}$ cm^{-3} [9]. This value indicates that the behaviour of the vacancy-related defects is comparable with that found in natural silicon. The contamination by hydrogen was studied with deep level transient spectroscopy; no hydrogen was found, to within the 2×10^{13} cm^{-3} detection limit [10].

The lattice expansion and contraction coefficients β, where $N_i \cdot \beta_i = \Delta a/a$, were measured at PTB by X-ray diffraction in significantly doped Si samples [11]. The measured β_i values are $-6.9(5) \times 10^{-24}$ cm^3 for carbon, $4.4(2) \times 10^{-24}$ cm^3 for oxygen [12], and $-5.6(2) \times 10^{-24}$ cm^3 for boron. For the vacancies, no significant influence on the lattice parameter could be found [13]. The investigations about lattice-parameter variations by X-ray topography showed no significant deviation ($\ll 10^{-8}a$) from homogeneous lattice spacing. Investigation with laser scattering tomography proved the absence of voids larger than the 30 nm detection limit [14]. The point-defect concentrations and concen-

tration differences necessary to extrapolate the mean lattice parameter of the spheres from that of the X-ray interferometer and to correct the sphere mass were obtained by polynomial interpolations; they are summarized in table 2.

Table 1. Impurity content N in the ^{28}Si crystal Si28-10Pr11. The increased amount of boron at the axial position near 420 mm was caused by a small crystal, grown by the Czochralski method from the residuals, joined on top to increase the length of the rod.

Axial distance from seed mm	Radial distance from centre mm	Sample SIS-code	N_C 10^{15} cm^{-3}	N_O 10^{15} cm^{-3}	N_B 10^{15} cm^{-3}
175.4	23	4.7.1	0.182(83)	0.196(23)	0.0196(17)
180.8	30	5A4.1.2	0.143(80)	0.206(20)	0.0202(17)
180.8	30	5A3.1.2	0.252(91)	0.217(19)	0.0206(17)
180.8	30	5A2.1.2	0.144(22)	0.216(19)	0.0210(18)
180.8	30	5A1.1.2	0.177(80)	0.213(19)	0.0199(17)
277.2	30	5B4.1.2	0.771(88)	0.265(27)	0.0033(7)
277.2	30	5B3.1.2	1.039(89)	0.352(33)	0.0052(7)
277.2	30	5B2.1.2	0.973(86)	0.321(32)	0.0062(8)
277.2	30	5B1.1.2	0.823(98)	0.333(30)	0.0059(8)
303.9	34	6.3.2	1.000(75)	0.366(32)	0.0029(5)
318.7	35	8A4.1.2	1.146(83)	0.383(34)	0.0036(5)
318.7	35	8A3.1.2	1.010(103)	0.384(34)	0.0016(6)
318.7	35	8A2.1.2	1.180(85)	0.399(35)	0.0036(5)
318.7	35	8A1.1.2	1.160(139)	0.399(35)	0.0064(7)
416.2	35	8B4.1.2	2.690(190)	0.434(38)	0.112(9)
416.2	35	8B3.1.2	2.540(182)	0.434(37)	0.107(9)
416.2	35	8B2.1.2	2.610(185)	0.433(38)	0.111(9)
416.2	35	8B1.1.2	2.740(193)	0.437(38)	0.187(15)
419.8	33	9.7.1	2.990(196)	0.440(38)	0.344(28)

Table 2a. Point defect concentration in the AVO28-S5 and AVO28-S8 spheres and in the X-ray interferometer (XINT) derived from a polynomial interpolation of the values listed in table 1.

Defect	Unit	AVO28-S5	AVO28-S8	XINT
Carbon	10^{15} cm^{-3}	0.40(5)	1.93(19)	1.07(10)
Oxygen	10^{15} cm^{-3}	0.283(63)	0.415(91)	0.369(33)
Boron	10^{15} cm^{-3}	0.011(4)	0.031(18)	0.004(1)
Vacancy	10^{15} cm^{-3}	0.33(11)	0.33(11)	0.33(11)

Table 2b. Differences of point defect concentrations in the AVO28-S5 and AVO28-S8 spheres with respect to the X-ray interferometer (XINT).

Defect	Unit	AVO28-S5 - XINT	AVO28-S8 - XINT
Carbon	10^{15} cm^{-3}	-0.67(8)	0.86(17)
Oxygen	10^{15} cm^{-3}	-0.086(59)	0.046(85)
Boron	10^{15} cm^{-3}	0.007(4)	0.027(18)
Vacancy	10^{15} cm^{-3}	0.00(11)	0.00(11)

2.2. *Molar mass*

The molar mass of silicon crystal material is given by

$$M = \Sigma_n M(^n\mathrm{Si})\, x_n = \Sigma_n M(^n\mathrm{Si})\, R_{n/m} \,/\, \Sigma_n R_{n/m}\,, \qquad (2)$$

where n = 28, 29, 30, $M(^n\mathrm{Si})$ is the molar mass of the silicon isotope ^{n}Si, x_n is the amount-of-substance fraction of ^{n}Si, $R_{n/m} = x_n / x_m$ are fraction ratios, and m labels the fraction chosen as a reference.

To determine the molar mass, a number of samples were taken from both sides of each sphere. High resolution measurements were carried out at the IRMM, by gas mass spectrometry (GMS) on the SiF_4 gas, and at the PTB, by isotope dilution combined with multicollector inductively coupled plasma mass spectrometry (IDMS). The repeatability and the uncertainty of both measurement are below 10^{-8}; however, the uncertainties do not overlap.

The main difference between the two methods is to be found in the chemical preparation of the samples. At the PTB, the ^{28}Si samples were dissolved in NaOH, whereas at IRMM they were dissolved in HF and converted into SiF_4 gas, via precipitation of the $BaSiF_6$ salt. The PTB measured only the amount-of-substance fractions of the ^{29}Si and ^{30}Si isotopes, both forming a virtual two-isotope element within the matrix of all the isotopes. The amount-of-substance fraction of the ^{28}Si isotope was obtained indirectly [15]. The spectrometer was calibrated on-line by using synthetic mixtures of natural Si and two crystals enriched with ^{29}Si and ^{30}Si isotopes. Natural Si contamination, memory effects due to previous measurements, and offsets were corrected on-line by bracketing each measurement of a sample, spike, blend, or mixture with blank – aqueous NaOH solutions – measurements. At IRMM, the natural Si contamination could not be measured on-line. An analysis of the solutions used to convert the crystal samples (carried out at the University of Warsaw by graphite-furnace atomic absorption spectroscopy) evidenced that, in the chemical processing of 50 mg ^{28}Si, about 8 µg natural Si were added by the chemical reagent used. This natural silicon contamination resulted in a very large correction of 62×10^{-8} *M*. Furthermore, the very high isotopic enrichment showed to be a big challenge; ion current ratios more than five orders of magnitude greater than unity had to be measured.

The isotopic composition of the ^{28}Si crystal was determined also at the Institute for Physics of Microstructures in Russia by a secondary ion mass spectrometer (SIMS) equipped with a time-of-flight mass analyzer. Gas mass spectrometry was also used at the Institute for Mineral Resources in China (IMR) via direct fluorination by BrF_5.

Figure 2 shows the measured ^{29}Si and ^{30}Si amount fractions [16]. The highest enrichments are observed by IDMS and SIMS. By continuous addition of natural Si to a material having the isotopic composition determined by IDMS, the ^{29}Si and ^{30}Si fractions moves along the black line and also passes near the other measurement results. Under this assumption of a natural Si contamination, the isotopic compositions determined by IDMS and by GMS are consistent with each other: The samples used for the GMS resulted unintentionally contaminated by natural silicon. Only the IRMM and PTB carried out calibrated measurements of the isotope amount ratios, but only the PTB assessed the total uncertainty budget. The analysis of measurement results indicates that: The data are consistent with a model which takes account of a natural Si contamination, with the PTB data being uncontaminated; The isotopic composition determined by the PTB is consistent with those determined by the IRMM, IMR, and IPM-RAS; No data set displays correlation between the measured isotopic composition and the sample location; The standard deviation and correlation of the PTB data-set are consistent with those associated with each individual datum. For this reasons, only the PTB data have been taken into account. A detailed data analysis substantiating this choice is given in [16], whereas the molar mass values and uncertainties used to calculate N_A are given in table 3 [17].

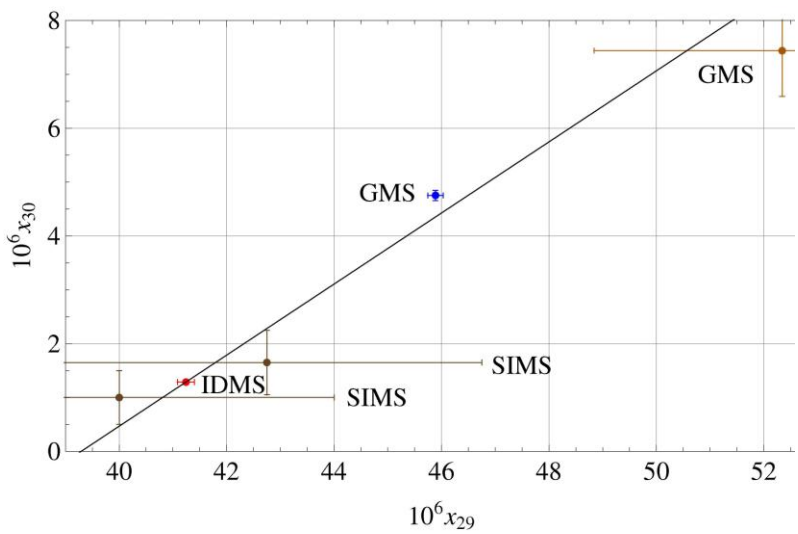

Figure 2. Isotope amount fractions of the enriched crystal. Measured isotope amount fractions x_{29} and x_{30} of the ^{28}Si boule as determined by gas mass spectrometry (GMS – brown, IMR, and blue, IRMM), by secondary ion mass spectrometry (SIMS), and isotope dilution mass spectrometry (IDMS). The solid line indicates the composition of fictional samples obtained by addition of natural silicon to the enriched sample measured by IDMS. Bars represent the standard uncertainties.

Table 3. Molar mass of the enriched Si material measured by IDMS.

Sample	Axial position/mm	*M*/(g/mol)
4.4	176	27.97697030(28)
5.B2.1.4	277	27.97697009(20)
5.B3.1.1.3	277	27.97697039(23)
5.B4.1.1.4	277	27.97697035(23)
Weighted mean AVO28-S5		27.97697026(15)
8.A2.1.4	319	27.97697006(24)
8.B4.1.1.3	416	27.97697047(24)
9.8	421	27.97697033(21)
Weighted mean AVO28-S8		27.97697029(16)

When averaging the data to calculate the molar mass of each sphere (table 3), data correlation was taken into account. Since each sample was separately dissolved into aqueous NaOH and since each measurement run was individually corrected for the background current and calibrated, correlations were small, about 20%. A detailed analysis of the molar mass measurements is given in [17]. No correlation between the isotopic composition of the samples and their location has been observed; the small relative 1×10^{-9} difference of the sphere molar mass confirms that the molar mass is the same in the whole crystal. However, since the molar mass was measured only in a few samples around the spheres, an additional uncertainty contribution due to a possible undetected maximum difference of 1×10^{-8} *M* between the crystal ends was temporarily taken into account (table 8).

2.3. Lattice parameter

The combined X-ray and optical interferometer used to determine the {220} lattice-plane spacing of silicon crystals at the INRIM was technologically improved and properly upgraded to expand measurement capabilities up to a few centimetre crystal-scan [18]. This made more numerous systematic effects visible and reproducible and it allowed wider crystal parts to be surveyed, thus increasing confidence in the crystal perfection and in the measured value of the lattice parameter. A set of lattice spacing values for different natural Si crystals were also re-measured, to ensure

a reliable link between enriched and natural crystals [19]. Next, a 6 cm long interferometer was manufactured from the material between the two ^{28}Si spheres. The mean lattice spacing value

$$d_{220}(\mathrm{XINT}) = a(\mathrm{XINT})/\sqrt{8} = 192.01471267(67)\ \mathrm{pm} \tag{3}$$

was measured at a distance of 306 mm from the seed crystal, t_{90} = 20 °C, and p = 0 Pa [20].

The mean lattice parameter of each sphere,

$$a(\mathrm{S}) = (1 + \Sigma_\mathrm{i}\, \beta_\mathrm{i}\, \Delta N_\mathrm{i})\, a(\mathrm{XINT}), \tag{4}$$

was calculated by taking account of the different point-defect concentrations in the spheres and the interferometer. In equation (4), S is the sphere AVO28-S5 or -S8, XINT is the X-ray interferometer, i labels the point defects, β_i is the strain coefficient, and ΔN_i the difference of the point-defect concentration between the sphere and the interferometer.

At the INRIM, the crystal perfection was checked along a 5 cm baseline. Figure 3 compares the lattice parameter values measured at 50 points 0.95 mm spaced along a 47 mm baseline. The measurements were carried out with the interferometer crystals assembled as they were in the ^{28}Si boule and also in a reversed alignment; no reproducible lattice strain has been detected, to within the present 3×10^{-9} resolution. Additional crystal-strain topography – on a different sample – was made with similar results at the NMIJ by means of a novel self-referenced X-ray diffractometer at the Photon Factory of the High Energy Accelerator Research Organization (KEK, Japan) [21].

Additional crystal samples were taken before, between, and after the ^{28}Si spheres. The NIST compared by double-crystal Laue diffractometry the lattice parameter of these samples against the parameter of a natural Si sample taken from the WASO04 crystal [22]. No significant difference of the measured lattice parameters from the values expected owing to impurity concentration was observed. Next, the NIST data were interpolated by application of a polynomial model of the impurity concentration along the axis of the ^{28}Si boule and, after the lattice parameter of the reference WASO04 sample was taken into account, an additional lattice spacing value at the distance of 306 mm from the seed crystal was obtained. The measurement results of the INRIM and NIST are compared in table 4; they are in excellent agreement and additionally confirm the crystal homogeneity.

Table 4. ^{28}Si (220) lattice spacing at t_{90} = 20 °C and in vacuum.

Axial position / mm	SIS code	d(220) / pm	Method
306*	–	192.01471275(119)	Lattice spacing comparison
306	6.5	192.01471267(67)	X-ray interferometry

*) The lattice spacing value at the 306 mm axial position was obtained by interpolation – according to a polynomial model of impurity concentrations – of the 36 values measured in the samples 4.5(A and B), 6.4(A and B), and 9.5(A and B).

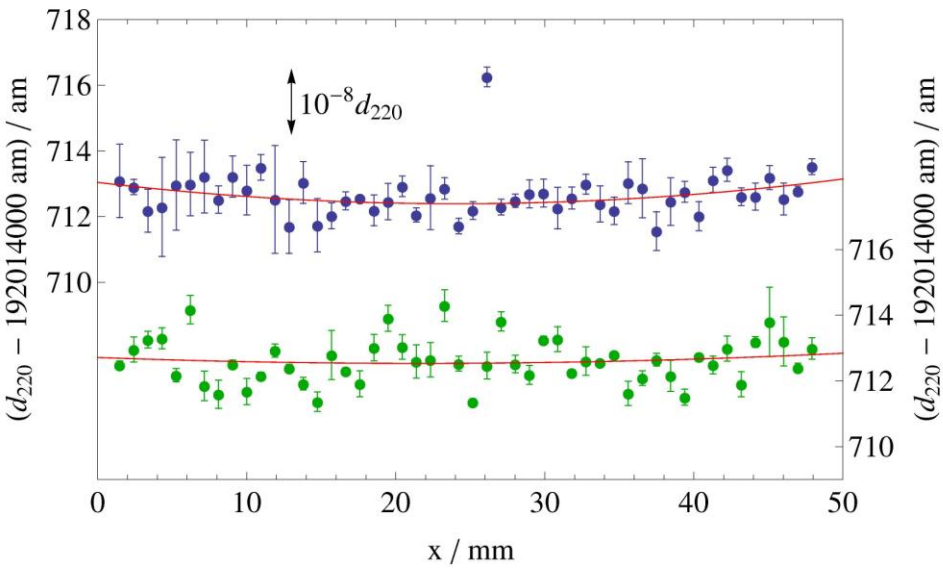

Figure 3. Map of the {220} lattice-plane spacing values along the same 5 cm baseline measured with the interferometer crystals assembled as they were in the ^{28}Si boule (top plot) or in the reversed alignment (bottom plot). Bars represent the standard deviation.

2.4. Surface

The thickness and the mass of the surface layer covering the 1 kg spheres must be taken into account when the silicon density is derived from mass and volume measurements. Mass, thickness and chemical composition of the surface layer were characterized by the following methods [23]: X-ray fluorescence analysis (XRF, in air and vacuum), near edge X-ray absorption fine structure spectroscopy (NEXAFS, vacuum), X-ray reflectometry (XRR, vacuum), X-ray photoelectron spectroscopy (XPS, vacuum), and optical spectral ellipsometry (SE, in air). For traceable determination of the oxide layer thickness, synchrotron radiation-based XRR at specific surface points had been chosen to calibrate the mapping by SE. By selecting photon energies around the oxygen K absorption edge at 543 eV, which energies are available at the PGM beamline of the PTB's laboratory at BESSY II [24], XRR is possible also for SiO_2 layers on much curved surfaces [25]. However, an unexpected metallic contamination (by copper and nickel) was detected on the sphere surfaces, which is limiting the total measurement uncertainty because of its significant influence on the optical constants of the sphere surface layer. NEXAFS measurements at the same beamline revealed that metallic contaminants are present as silicides. Therefore, the direct oxide thickness determination by XRR at the oxygen K-edge on the sphere was replaced by XRF measurements, in which the oxygen K fluorescence intensity from the sphere surface was compared with that from flat samples, for which the oxide layer thickness was determined by XRR.

The surface layer of the spheres was divided for data evaluation into four sub-layers; from top to bottom: a carbonaceous contamination layer (CL) [26], a chemisorbed water layer (CWL), a layer of metallic silicides (ML) and a pure oxide layer (OL). The mass deposition of the metallic contamination and of carbon was also derived from XRF measurements by synchrotron radiation by comparison to flat reference samples having a layer thickness determined by XRR. XPS was used to investigate the stoichiometry of the oxide layer. In addition, XPS gave also a rough determination of the oxide-layer thickness, which was found to be in good agreement with the values measured by XRF/XRR combination. At NMIJ, the ellipsometer data were calibrated by SiO_2 layers on wafers with thicknesses certified by XRR measurements.

The apparent thickness of the carbonaceous layer (CL) was measured on eight spheres at BESSY by XRF in a comparison with a reference sample having a 6.5 nm carbon layer; the result is 0.212(39) nm, on the average and on the assumption of the same density as that of the reference. This apparent thickness is consistent with the expected residual carbonaceous contamination due to the sphere-cleaning procedure applied. Since the carbonaceous contamination depends on a large set of environmental parameter (humidity, residual gas concentration, etc.), the exact amount of contamination is measured for each sphere simultaneously to the thickness determination. With an esti-

mated density of 1.0(2) g/cm^3, a mass of m_{CL} = 15.0(3.8) µg for AVO28-S5 and of m_{CL} = 13.1(3.3) µg for AVO28-S8 was derived for the carbonaceous layer. The associated thicknesses are: d_{CL} = 0.54(18) nm (AVO28-S5) and d_{CL} = 0.47(16) nm (AVO28-S8).

For mass deposition of the chemisorbed water monolayer (CWL), which is the residual water on the sphere under vacuum conditions, the value 0.028(4) µg/cm^2 measured by Mizushima [27] was applied. To account for the difference between the characteristics of the wafer and the sphere surfaces, the uncertainty of the Mizushima's value was increased by a factor of two. A 1.0(1) g/cm^3 density of the water layer was assumed. The corresponding layer mass and thickness are 7.7(2.2) µg and 0.28(8) nm, respectively. A physical adsorbed water layer (PWL) has to be taken into account only if measurements are carried out in air, which is the case in the oxide thickness determination at NMIJ (see below).

The Ni, Cu, and Zn depositions and their binding characteristics were measured by XRF, NEXAFS, and XPS [23]. The chemical compositions $NiSi_x$, $CuSi_x$, $ZnSi_x$, with x = 1.0(1), were used to calculate the mass of the layer. A density of 7.2(2.0) g/cm^3 of this layer was estimated (results in 5).

The stoichiometry of the oxide layer (OL) was measured by XPS [28]; a pure SiO_2 layer was found. At PTB, the total oxygen surface-content was measured by XRF by comparison with a set of SiO_2 reference samples, having thickness between 2 nm and 10 nm and calibrated by XRR measurements. A 2.2(1) g/cm^3 oxide density was assumed. Eventually, for observation in detail of the variation of the oxide layer thickness, SE was applied to map the whole surface-layer and to generate a complete topography consisting of about 5500 data points (figure 4). At the NMIJ, a spectroscopic ellipsometer was calibrated by means of SiO_2 layers on Si wafers having thicknesses certified by a traceable XRR system. In the evaluation of the ellipsometric data measured at the points distributed uniformly over the surface of the sphere, an additional physisorbed water layer (PWL) had to be considered, because the ellipsometric measurement was made in air. By use of a five-layer model, the thickness of the SiO_2 layer was evaluated from the SE data by taking account of the optical constants of each layer [23]. The thicknesses of all other layers determined by XRF at PTB and the mass measurements at NMIJ were used in the NMIJ evaluation.

Contrary to the model introduced by Seah et al. [26], a SiO intermediate layer was not detected by the XPS measurements; an upper limit of d_{SiO} = 0.05 nm was derived, so that correction to the density determination is negligible. The overall surface layer thickness d_{SL} is the sum of d_{CL} + d_{CWL} + d_{ML}+ d_{OL}, and the layer mass was calculated accordingly. The individual thicknesses and masses of the sublayers and those of the overall surface-layer for the two spheres are given in tables 5a and 5b.

Table 5a. Thickness of surface layer and sub-layers.

Sphere	Lab.	d_{CL}/nm	d_{CWL}/nm	d_{ML}/nm	d_{OL}/nm	d_{SL}/nm
AVO28-S5	PTB	0.54(18)	0.28(8)	0.54(16)	1.55(22)	2.91(34)
	NMIJ				1.36(52)	
	average				1.52(20)	2.88(33)
AVO28-S8	PTB	0.47(16)	0.28(8)	0.54(17)	1.42(22)	2.71(33)
	NMIJ				1.28(51)	
	average				1.40(20)	2.69(32)

Table 5b. Mass of surface layer and sub-layers.

Sphere	m_{CL}/µg	m_{CWL}/µg	m_{ML}/µg	m_{OL}/µg	m_{SL}/µg
AVO28-S5	15.0(3.8)	7.7(2.2)	107.1(5.2)	92.3(12.8)	222.1(14.5)
AVO28-S8	13.1(3.3)	7.7(2.2)	107.8(5.5)	85.0(12.7)	213.6(14.4)

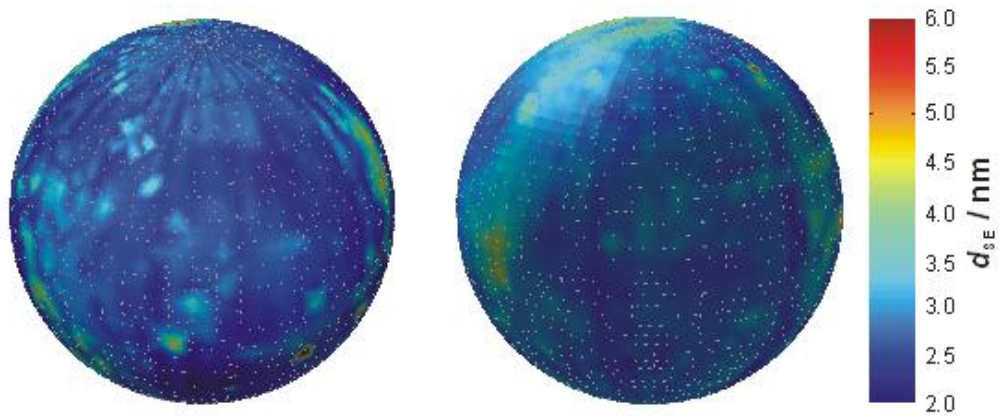

Figure 4. Topographic maps of the surface layer thickness measured by spectral ellipsometry (not calibrated). Left AVO28-S5, right AVO28-S8. The rainbow colour code ranges from 2.0 nm (blue) to 4.5 nm (yellow).

2.5. Volume

The volumes of six 1 kg spheres of natural and enriched silicon were determined by means of two different optical interferometers. The general procedure is based on a differential measurement: Both interferometers consist of a stable étalon – in one case being two confocal spherical plates; in the other, being a pair of parallel flat optical plates. Firstly, the étalon dimension D was determined. Then, the sphere was placed between the plates and the two gaps d_1 and d_2 between the sphere and the relevant plate were determined. The sphere diameter is $d = D - d_1 - d_2$. Tuneable diode lasers traced back to iodine stabilised lasers were used to evaluate the interference-pattern fractions with a wavelength tuning technique. The interference patterns were acquired by high dynamic cameras allowing application of sophisticated algorithms for image processing. In the case of the NMIJ plane étalon, the interference pattern shows concentric fringes, the central order of which must be determined; the measurement result is a single diameter value. Differently, in both the configurations of the PTB spherical interferometer, empty étalon and loaded with the sphere, the interference pattern are equal thickness fringes in the full field of view. This made it possible to determine one diameter for each camera pixel and a complete topographical mapping of both spheres [29] (figure 5).

The NMIJ measured several hundred diameters. The main improvements were the reconfiguration of the optical interferometer to eliminate the phase errors due to the diffraction by the optical components, the evaluation of the effect of the Gouy phase-shift on the diameter measurement, the installation of an active radiation shield to reduce uncertainty in the sphere temperature measurement, and the improved evaluation of the interferogram phase-profile [30,31,32,33,34]. A detailed analysis outlined a model of the NMIJ interferometer operations to quantify and to minimize the corrections of the effect of the Gouy phase shift to the diameter measurements [35]. A comparison of diameter measurements between NMIJ and PTB with use of a natural Si sphere named AVO#3 demonstrated excellent agreement within the measurement uncertainty [36].

The optical constants of the different surface layers and the resulting phase shift correction $\Delta\phi_0$ were calculated from the thickness values given in table 5a [29]. The optical constants concerning the metallic contamination, n_r = 2.67(20) and k = 2.75(20), are dominating the uncertainty budget of the phase correction $\Delta\phi_0$.

In table 6 are summarized the diameter measurements and the phase shift corrections with the use of both types of interferometers. Calculations show that the influence of the surface layer on the optical diameter measurements is very small [29].

Table 6. Diameter and volume of enriched Si spheres (t_{90} = 20 °C , vacuum).

Sphere	Lab.	Mean apparent diameter/µm	$2\Delta\Phi_0$/nm	Mean diameter of Si core/µm	Volume V of Si core/cm^3

AVO28-S5	PTB	93722.9717(11)			
AVO28-S5	NMIJ	93722.9726(16)			
AVO28-S5 weighted mean		93722.9720(9)	0.07(15)	93722.9721(9)	431.059061(13)
AVO28-S8	PTB	93722.2510(8)			
AVO28-S8	NMIJ	93722.2505(14)			
AVO28-S8 weighted mean		93722.2509(7)	0.03(15)	93722.2509(7)	431.049111(10)

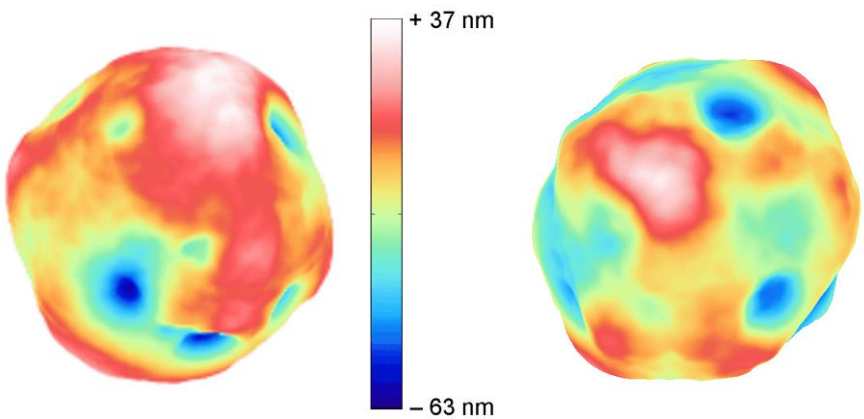

Figure 5. Diameter topographies of the silicon spheres. Peak-to-valley distances are 98 nm (AVO28-S5, left) and 90 nm (AVO28-S8, right).

2.6. Mass

Mass comparisons of the two ^{28}Si spheres with Pt-Ir kilogram standards were carried out at the BIPM, NMIJ, and PTB [37]. Suitable vacuum mass comparators have been available since a few years ago, which make it possible to determine the mass of 1 kg silicon spheres under vacuum conditions (10^{-3} Pa to 0.1 Pa). Owing to the air-to-vacuum transfers of the reference standards, sorption corrections had to be considered, which were determined by means of sorption artefacts. The results are in excellent agreement and demonstrate an accuracy below 5 µg in the mass determination (figure 6 and table 7).

To determine the mass of the silicon core, the mass of the surface layers, including the metallic contaminations, was subtracted from the mass of the sphere. In addition, owing to point defects, there is a

$$m_{\mathrm{deficit}} = V \sum_{\mathrm{i}} (m_{28} - m_{\mathrm{i}}) N_{\mathrm{i}} \qquad (5)$$

difference between the mass of a sphere having Si atoms on all regular sites and the measured mass value. In equation (5), m_{28} and m_{i} are the masses of, respectively, a ^{28}Si atom and of the i-th point defect (a vacancy mass is zero and oxygen is associated with an interstitial lattice site, so that m_{O} is the sum of oxygen and ^{28}Si masses), V is the sphere volume, and N_{i} is the concentration of the i-th point defect. Thus, a mass deficit of 8.1(2.4) µg was calculated for the AVO28-S5 and a mass deficit of 24.3(3.3) µg for AVO28-S8.

After the surface-layer mass was subtracted and the mass deficit was added, the Si-core mass $m = m_{\mathrm{sphere}} - m_{\mathrm{SL}} + m_{\mathrm{deficit}}$ is obtained (table 7). Additional details about data analysis and averaging, as well as details about the impact of correlations – all mass measurements are traceable to the mass of the international prototype – are given in [37].

Table 7. Masses of the ^{28}Si spheres as measured in vacuum.

Sphere	Laboratory	Mass/kg	Date of measurement

AVO28-S5	NMIJ	1.000 087 771 8(166)	06/2008
AVO28-S5	BIPM	1.000 087 773 7(54)	10/2008
AVO28-S5	PTB	1.000 087 765 4 (130)	03/2009
AVO28-S5	BIPM	1 000 087 776 2(54)	09/2009
AVO28-S5	Weighted mean	1.000 087 772 4(41)	
AVO28-S8	BIPM	1.000 064 730 8(54)	11/2008
AVO28-S8	NMIJ	1.000 064 712 6(166)	02/2009
AVO28-S8	BIPM	1.000 064 737 1(54)	09/2009
AVO28-S8	PTB	1.000 064 730 4(65)	02/2010
AVO28-S8	Weighted mean	1.000 064 7307(41)	

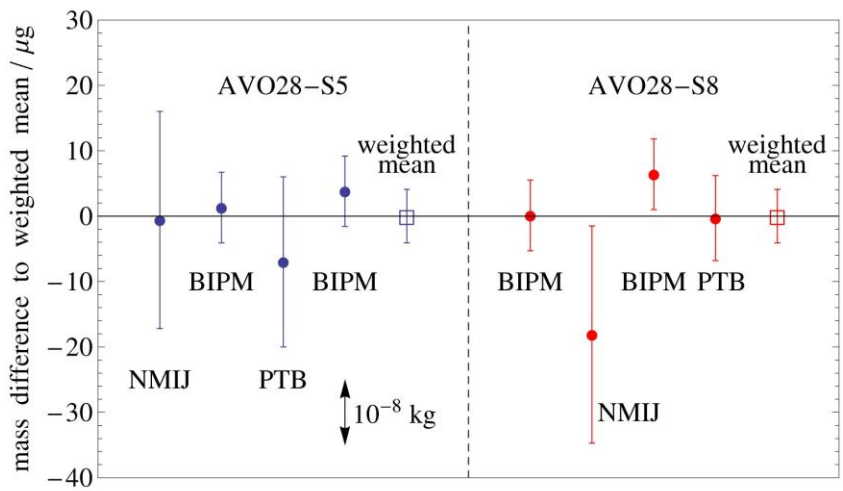

Figure 6. Masses of the silicon spheres AVO28-S5 and AVO28-S8 weighed in vacuum by BIPM, NMIJ, and PTB. The absolute mass difference between the two spheres is $m_{S5} - m_{S8}$ = 23.042 mg. Bars represent the standard uncertainties.

2.7. Density

The density of each silicon sphere is calculated from the diameter of its core (table 6), the thickness of its surface layer (table 5), and the mass of the whole sphere (table 7); the results are 2320.070 909(84) kg/m^3 for AVO28-S5 and 2320.071 038(72) kg/m^3 for AVO28-S8. The density difference between the two spheres was measured by the pressure-of-flotation method [38,39], the relative differences measured by the NMIJ [40] and PTB [29] are 26(9) × 10^{-9} and 20(10) × 10^{-9}, respectively. This difference agrees with the 56(33) × 10^{-9} relative density difference calculated from the absolute measurements. It can be explained by the different impurity concentrations in the two spheres, which difference yields a 14(4) × 10^{-9} relative density difference. This further agreement with the density difference expected from the impurity concentration difference also indicates that imperfections in the crystal structure causing relative density differences larger than 10^{-8} are unlikely.

3. Avogadro constant

Table 8 gives the results of the measurements of molar mass, lattice parameter, thickness and mass of the surface layer, volume, mass, and density of the enriched silicon spheres. As is shown in table 9, the accuracy is limited by the not well known influence of the metallic contamination on the optical constants of the surface layer and by the influence of imperfect optical wave fronts in the measurements of the sphere diameters. For the evaluation and expression of measurement uncertainties the procedure suggested by the Guide to the Expression of Uncertainty in Measurement [41] was applied using the GUMWorkbench software [42]; covariances were calculated and taken into

account. The model equations and the list of quantities involved can be found in appendices A and B. The quantities dominating the total uncertainty are the apparent diameter, D_m, and the mass of the surface layer, m_{SL}.

The N_A determinations based on two spheres are summarized in table 8; they differ only by 37(35) × 10^{-9} N_A, thus confirming the crystal homogeneity. By averaging these values and multiplying the uncertainty with the Birge-ratio of 1.06, the final value of the Avogadro constant is

$$N_A = 6.022\ 140\ 82(18) \times 10^{23}\ \mathrm{mol}^{-1}, \tag{6}$$

with a relative uncertainty of 3.0 × 10^{-8}.

Table 8. N_A determination. Lattice parameter, volume, and density are measured at t_{90} = 20.0 °C and p = 0 Pa.

Quantity	Unit	AVO28-S5	AVO28-S8
M	g/mol	27.97697026(22)	27.97697029(23)
a	pm	543.0996240(19)	543.0996185(20)
V	cm^3	431.059061(13)	431.049111(10)
m	g	1000.087558(15)	1000.064541(15)
$\rho = m/V$	kg/m^3	2320.070841(76)	2320.070998(64)
N_A	10^{23} mol^{-1}	6.022 140 95(21)	6.022 140 73(19)

Table 9. Uncertainty budget of the N_A determination by AVO28-S5 (compare Appendix C). The percent contributions to the total uncertainty are the relevant variance fractions with respect to the total variance. The main contributions are at present due to surface characterization and the volume determination.

Quantity	Relative uncertainty/10^{-9}	Contribution/%
Molar mass	8	5
Lattice parameter	11	9
Surface	15	18
Sphere volume	29	66
Sphere mass	4	1
Point defects	3	1
Total	36	100

4. Conclusions

Fifty years ago, Egidi [43] thought about obtaining an atomic mass standard. In 1965, Bonse and Hart [44] made the first X-ray interferometer, thus paving the way to the achievement of this dream, and soon Deslattes [45] completed the first N_A determination by counting the atoms in a natural silicon crystal. We concluded the project by carrying out a very accurate N_A measurement with the use of a silicon crystal highly isotopically enriched.

Table 10. Value of the Avogadro constant based on isotopically enriched silicon

Sphere	$N_A/10^{23}$ mol^{-1}	$u_r/10^{-9}$	Relative difference to CODATA 2006
AVO28-S5	6.022 140 95(21)	36	-0.14 × 10^{-6}
AVO28-S8	6.022 140 73(19)	32	-0.18 × 10^{-6}
Mean value	6.022 140 82(18)	30	-0.16 × 10^{-6}
CODATA 2006	6.022 141 79(30)	50	

The measurement uncertainty is 1.5 times higher than that targeted for a kilogram redefinition, but "close to the finish line of the marathon effort to tie the kilo to a constant of nature" [46]. The measurement accuracy seems to be limited by the working apparatuses. In fact, we have not detected clear effects of crystal imperfections, with respect to the measurement uncertainties obtained. To achieve the desired uncertainty we are planning to use improved optical interferometers, at present under test. Investigations are also under way to eliminate contamination from the sphere surfaces, without jeopardizing the excellent roundness and nano-roughness of the spheres, which are both essential for accurate density measurements. Investigations are in progress to identify the source of natural Si contamination occurring in gas mass spectrometry, and repetitions of the molar mass measurement will be carried out in other laboratories.

For the first time a comparison can be made of accurate values of the Planck constant derived from different experiments. This comparison is a test for the consistency of atomic physics. A parallel experiment, having the purpose of measuring $N_A h$ by absolute nuclear spectroscopy, is aiming at extending this test to nuclear physics [47]. Figure 7 shows our result compared with those of the two most accurate measurements so far carried out: the watt-balance experiments of the National Institute of Standards and Technology (NIST - USA) [48,49] and the National Physical Laboratory (NPL - UK) [50]. The values of the Planck constant measured by these experiments were converted into the corresponding N_A values by $N_A h$ = 3.990 312 6821(57) × 10^{-10} Js/mol, which has a relative uncertainty of 1.4 × 10^{-9} [51].

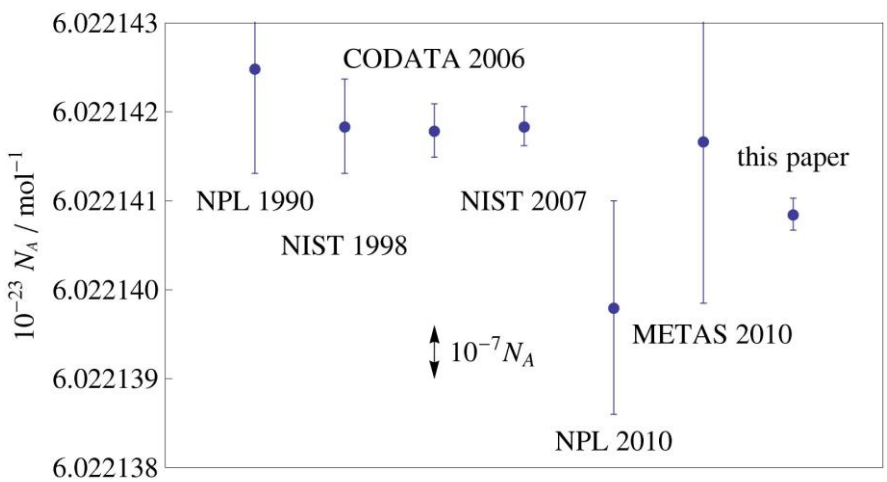

Figure 7. Avogadro constant determinations: Comparison between the most accurate N_A values at present available. Bars represent the standard uncertainty.

By significantly reducing existing discrepancies the present result leads to a more consistent set of numerical values for the fundamental physical constants. This result is also a significant step towards demonstrating a successful *mise en pratique* of a kilogram definition based on a fixed value of the Avogadro constant or of the Planck constant. The agreement between the different realizations is not yet as good as is required to withdraw the Pt-Ir kilogram prototype, but considering the capabilities already developed and the envisaged improvements, it seems realistic to achieve the targeted uncertainty in the foreseeable future [52].

Our results need to be completed by additional activities. One is to relate the mass of the ^{28}Si atom to its Compton's wavelength to test the mass-energy-frequency equivalence. Another is to monitor the stability of the Pt-Ir prototype: the technologies we developed can be refined and finalized to calculate the mass variation of 1 kg ^{28}Si-spheres by monitoring their surface evolution without weighing them on a balance. The last activity is to determine the mass of a ^{28}Si sphere by electrical measurements using a watt balance and without reference to the Pt-Ir prototype. In this

framework, it will be also necessary to demonstrate the mutual consistency and the stability of both the electrical and crystal *mise en pratique* of a kilogram definition based on a conventional value of the Planck constant. A related issue is the development of suitable procedures and protocols to disseminate the unit from the new realizations.

Acknowledgements
We wish to thank H.-J. Pohl for his outstanding encouragement, A. K. Kaliteevski and his colleagues at the Central Design Bureau of Machine Building and the Institute of Chemistry of High-Purity Substances for their dedicating work and the punctual delivering of the enriched material, H. Riemann and his staff from the Institut für Kristallzüchtung for the final crystal growth, our directors for their advice and generous financial support, and our colleagues for their daily work. This research received funds from the European Community's 7th Framework Programme ERA-NET Plus (grant 217257) and the International Science and Technology Centre (grant 2630).

Appendix

Appendix A. Model equations

$N_A = n\, M / (\rho\, V_0)$,

$V_0 = a_s^3$,

$a_{XINT} = d_{XINT} \sqrt{8}$,

$a_s = a_{XINT}\, (1 + \Delta a_{imp}/a)$,

$\Delta a_{imp}/a = \beta_C\, \Delta N_C + \beta_O\, \Delta N_O + \beta_B\, \Delta N_B + \beta_V\, \Delta N_V$,

$\rho = m / V$,

$V = \pi\, D_{core}^3 / 6$,

$D_{core} = D_m + 2\, \Delta \Phi_0$,

$m = m_{sphere} - m_{SL} + m_{deficit}$,

$m_{deficit} = m_{dB} + m_{dC} + m_{dO} + m_{dV}$,

$m_{dB} = V\, (A_{rSi} - A_{rB})\, N_B$ u,

$m_{dC} = V\, (A_{rSi} - A_{rC})\, N_C$ u,

$m_{dO} = -V\, A_{rO}\, N_O$ u,

$m_{dV} = V\, A_{rSi}\, N_V$ u.

Appendix B. List of quantities

Quantity	Unit	Definition
A_{rB}	1	Relative atomic mass of boron
A_{rC}	1	Relative atomic mass of carbon
A_{rO}	1	Relative atomic mass of oxygen
A_{rSi}	1	Relative atomic mass of silicon-28
a_s	m	Lattice parameter of the sphere at t_{90} = 20 °C and p = 0 Pa, not corrected for impurities
a_{XINT}	m	Lattice parameter of the X-ray interferometer at t_{90} = 20 °C and p = 0 Pa, not corrected for impurities

Quantity	Unit	Definition
D_{core}	m	Diameter of the sphere core at t_{90} = 20 °C and p = 0 Pa
D_m	m	Measured (apparent) diameter of the sphere at t_{90} = 20 °C and p = 0 Pa
d_{XINT}	m	Measured value of the {220} lattice-plane spacing at axial the position 306 mm (XINT), t_{90} = 20 °C and p = 0 Pa
m	kg	Mass of the sphere core, corrected for impurities and vacancies
M	kg/mol	Measured molar mass of the sphere
m_{dB}	kg	Mass deficit of the sphere due to boron
m_{dC}	kg	Mass deficit of the sphere due to carbon
$m_{deficit}$	kg	Mass deficit of the sphere due to impurities (B, C, O) and vacancies
m_{dO}	kg	Mass deficit of the sphere due to oxygen
m_{dV}	kg	Mass deficit of the sphere due to vacancies
m_{SL}	kg	Mass of surface layers on the sphere (in vacuum)
m_{sphere}	kg	Measured value of the sphere mass in vacuum (including surface layers)
n	1	Number of atoms in an ideal unit cell (= 8 exactly)
N_A	mol^{-1}	Avogadro constant
N_B	m^{-3}	Number density of boron atoms in the sphere
N_C	m^{-3}	Number density of carbon atoms in the sphere
N_O	m^{-3}	Number density of oxygen atoms in the sphere
N_V	m^{-3}	Number density of vacancies in the sphere
u	kg	Unified atomic mass unit
V	m^3	Volume of the sphere core at t_{90} = 20 °C and p = 0 Pa
V_0	m^3	Unit cell volume
β_B	m^3	Lattice parameter sensitivity to boron concentration
β_C	m^3	Lattice parameter sensitivity to carbon concentration
β_O	m^3	Lattice parameter sensitivity to oxygen concentration
β_V	m^3	Lattice parameter sensitivity to vacancy concentration
$\Delta a_{imp}/a$	1	Relative lattice parameter difference between the sphere and X-ray interferometer
ΔN_B	m^{-3}	Difference of number density of boron atoms between the sphere and X-ray interferometer
ΔN_C	m^{-3}	Difference of number density of carbon atoms between sphere and X-ray interferometer
ΔN_O	m^{-3}	Difference of number density of oxygen atoms between sphere and X-ray interferometer
ΔN_V	m^{-3}	Difference of number density of vacancies between sphere and X-ray interferometer
$\Delta \Phi_0$	m	Phase correction
ρ	kg/m^3	Density of silicon core of the sphere at t_{90} = 20 °C and p = 0 Pa (mass deficit corrected)

Appendix C. Uncertainty budget (for AVO28-S5)

Intermediate values have no own uncertainty contributions. Owing to the first order propagation of uncertainty, the sensitivity coefficients of the β_V and ΔN_V uncertainties are zero; the relevant uncertainty contributions are negligible.

Quantity	Value	Standard uncertainty	Degrees of freedom	Sensitivity coefficient	Uncertainty contribution	
					absolute	relative
A_{rB}	10.81100	$7.00 \cdot 10^{-3}$	50	$4.7 \cdot 10^{12}$	$33 \cdot 10^{9}$ mol^{-1}	0.0%

Quantity	Value	Standard	Degrees of	Sensitivity	Uncertainty contribution	
A_{rC}	12.010700	$800\cdot10^{-6}$	50	$170\cdot10^{12}$	$140\cdot10^{9}$ mol^{-1}	0.0%
A_{rO}	15.999400	$300\cdot10^{-6}$	50	$120\cdot10^{12}$	$37\cdot10^{9}$ mol^{-1}	0.0%
A_{rSi}	27.9800	0.0100	50	$-320\cdot10^{12}$	$-3.2\cdot10^{12}$ mol^{-1}	0.0%
a_s	$543.09962400\cdot10^{-12}$ m	$1.93\cdot10^{-18}$ m				
a_{XINT}	$543.09962171\cdot10^{-12}$ m	$1.90\cdot10^{-18}$ m				
D_{core}	0.093722972070 m	$912\cdot10^{-12}$ m				
D_m	0.093722972000 m	$900\cdot10^{-12}$ m	50	$19\cdot10^{24}$	$17\cdot10^{15}$ mol^{-1}	65.8%
d_{XINT}	$192.014712670\cdot10^{-12}$ m	$670\cdot10^{-21}$ m	50	$-9.4\cdot10^{33}$	$-6.3\cdot10^{15}$ mol^{-1}	8.7%
m	1.0000875585 kg	$15.3\cdot10^{-9}$ kg				
M	0.027976970260 kg/mol	$220\cdot10^{-12}$ kg/mol	50	$22\cdot10^{24}$	$4.7\cdot10^{15}$ mol^{-1}	4.9%
m_{dB}	$135.2\cdot10^{-12}$ kg	$49.2\cdot10^{-12}$ kg				
m_{dC}	$4.572\cdot10^{-9}$ kg	$572\cdot10^{-12}$ kg				
$m_{deficit}$	$8.08\cdot10^{-9}$ kg	$2.39\cdot10^{-9}$ kg				
m_{dO}	$-3.241\cdot10^{-9}$ kg	$721\cdot10^{-12}$ kg				
m_{dV}	$6.61\cdot10^{-9}$ kg	$2.20\cdot10^{-9}$ kg				
m_{SL}	$222.0\cdot10^{-9}$ kg	$14.5\cdot10^{-9}$ kg	50	$600\cdot10^{21}$	$8.7\cdot10^{15}$ mol^{-1}	16.7%
m_{sphere}	1.00008777240 kg	$4.10\cdot10^{-9}$ kg	50	$-600\cdot10^{21}$	$-2.5\cdot10^{15}$ mol^{-1}	1.3%
n	8.0					
N_B	$11.00\cdot10^{18}$ m^{-3}	$4.00\cdot10^{18}$ m^{-3}	50	$-7.4\cdot10^{-6}$	$-30\cdot10^{12}$ mol^{-1}	0.0%
N_C	$400.0\cdot10^{18}$ m^{-3}	$50.0\cdot10^{18}$ m^{-3}	50	$-6.9\cdot10^{-6}$	$-340\cdot10^{12}$ mol^{-1}	0.0%
N_O	$283.0\cdot10^{18}$ m^{-3}	$63.0\cdot10^{18}$ m^{-3}	50	$6.9\cdot10^{-6}$	$430\cdot10^{12}$ mol^{-1}	0.0%
N_V	$330\cdot10^{18}$ m^{-3}	$110\cdot10^{18}$ m^{-3}	50	$-12\cdot10^{-6}$	$-1.3\cdot10^{15}$ mol^{-1}	0.4%
u	$1.6605387820\cdot10^{-27}$ kg	$83.0\cdot10^{-36}$ kg	50	$-2.9\cdot10^{42}$	$-240\cdot10^{6}$ mol^{-1}	0.0%
V	$431.0590612\cdot10^{-6}$ m^3	$12.6\cdot10^{-12}$ m^3				
V_0	$160.19114528\cdot10^{-30}$ m^3	$1.71\cdot10^{-36}$ m^3				
β_B	$-5.600\cdot10^{-30}$ m^3	$200\cdot10^{-33}$ m^3	50	$-13\cdot10^{42}$	$-2.5\cdot10^{12}$ mol^{-1}	0.0%
β_C	$-6.900\cdot10^{-30}$ m^3	$500\cdot10^{-33}$ m^3	50	$1.2\cdot10^{45}$	$610\cdot10^{12}$ mol^{-1}	0.1%
β_O	$4.400\cdot10^{-30}$ m^3	$200\cdot10^{-33}$ m^3	50	$160\cdot10^{42}$	$31\cdot10^{12}$ mol^{-1}	0.0%
β_V	0.0 m^3	$1.00\cdot10^{-30}$ m^3	50	0.0	0.0 mol^{-1}	0.0%
$\Delta a_{imp}/a$	$4.205\cdot10^{-9}$	$697\cdot10^{-12}$				
ΔN_B	$7.00\cdot10^{18}$ m^{-3}	$4.00\cdot10^{18}$ m^{-3}	50	$10\cdot10^{-6}$	$40\cdot10^{12}$ mol^{-1}	0.0%
ΔN_C	$-670.0\cdot10^{18}$ m^{-3}	$80.0\cdot10^{18}$ m^{-3}	50	$12\cdot10^{-6}$	$1.0\cdot10^{15}$ mol^{-1}	0.2%
ΔN_O	$-86.0\cdot10^{18}$ m^{-3}	$59.0\cdot10^{18}$ m^{-3}	50	$-7.9\cdot10^{-6}$	$-470\cdot10^{12}$ mol^{-1}	0.0%
ΔN_V	0.0 m^{-3}	$110\cdot10^{18}$ m^{-3}	50	0.0	0.0 mol^{-1}	0.0%
$\Delta\Phi_0$	$35.0\cdot10^{-12}$ m	$75.0\cdot10^{-12}$ m	50	$39\cdot10^{24}$	$2.9\cdot10^{15}$ mol^{-1}	1.8%
π	3.1415926535898					
ρ	2320.0708405 kg/m^3	$76.4\cdot10^{-6}$ kg/m^3				
N_A	$602.214095\cdot10^{21}$ mol^{-1}	$21.4\cdot10^{15}$ mol^{-1}	110			

References

[1] Becker P 2001 History and progress in the accurate determination of the Avogadro constant *Rep. Prog. Phys.* **64** 1945-2008

[2] Mills I M, Mohr P J, Quinn T J, Taylor B N and Williams E R 2006 Redefinition of the kilogram, ampere, kelvin and mole: a proposed approach to implementing CIPM recommendation 1 (CI-2005) *Metrologia* **43** 227-246

[3] Kibble B P 1976 A measurement of the gyromagnetic ratio of the proton by the strong field method *Atomic Masses and Fundamental Constants* **5** ed Sanders J H and Wapstra A H (New York: Plenum) 545-551

[4] Zosi G 1983 A neo-Pythagorean approach towards an atomic-mass standard *Lettere al Nuovo Cimento* **38** 577-580

[5] Mohr P J and Taylor B N 2000 CODATA recommended values of the fundamental physical constants: 1998 *Rev. Mod. Phys.* **72** 351-495

[6] Becker P *et al* 2006 Large-scale production of highly enriched ^{28}Si for the precise determination of the Avogadro constant *Meas. Sci. Technol.* **17** 1854-1860

[7] Yang A *et al* 2009 Simultaneous Subsecond Hyperpolarization of the Nuclear and Electron Spins of Phosphorus in Silicon by Optical Pumping of Exciton Transitions *Phys. Rev. Lett.* **102** 257401-1-4

[8] Zakel S, Wundrack S, Niemann H, Rienitz O and Schiel D 2011 Infrared spectrometric measurement of impurities in highly enriched "^{28}Si", in prep. for *Metrologia*

[9] Krause-Rehberg R 2008 Laboratory report, University Halle-Wittenberg, Germany

[10] Lavrov E 2010 Laboratory report TU Dresden, Germany

[11] Zulehner W 1991 in: *Landoldt-Börnstein New Series* **III/22b**, Hellwege K H and Madelung M, Eds. Berlin: Springer-Verlag 394

[12] Becker P and Windisch D 1990 Silicon lattice spacings as an absolute scale of length for high precision measurements of fundamental constants *Phys. Stat. Sol.* **a118** 379-388

[13] Martin J 1998 Ist Silicium zur Neudefinition des Kilogramms geeignet? *PTB-report* APh-28 Physikalisch-Technische Bundesanstalt Braunschweig, Germany

[14] Riemann H 2008 Laboratory report, Leibniz Institut für Kristallzüchtung Berlin, Germany

[15] Rienitz O, Pramann A and Schiel D 2010 Novel concept for the mass spectrometric determination of absolute isotopic abundances with improved measurement uncertainty: Part 1 – theoretical derivation and feasibility study *Int. J. Mass Spectrom.* **289** 47-53

[16] Bulska E, Drozdov M N, Mana G, Pramann A, Rienitz O, Sennikov P and Valkiers S 2011 The isotopic composition of enriched Si: a data analysis, in prep. for *Metrologia*

[17] Pramann A, Rienitz O, Schiel D, Schlote J, Güttler B and Valkiers S 2011 Molar mass of silicon highly enriched in ^{28}Si determined by IDMS, in prep. for *Metrologia*

[18] Ferroglio L, Mana G and Massa E 2008 Si lattice parameter measurement by centimeter x-ray interferometry *Opt. Express* **16** 6877-88

[19] Massa E, Mana G, Kuetgens U and Ferroglio L 2009 Measurement of the Lattice Parameter of a Silicon Crystal *New J. Phys.* **11** 053013

[20] Massa E, Mana G, Kuetgens U and Ferroglio L 2010 Measurement of the {220} lattice plane spacing of a ^{28}Si crystal *Metrologia* submitted

[21] Fujimoto H, Waseda A and Zhang X, Homogeneity characterization of lattice spacing of silicon single crystals by the self-referenced lattice comparator, in prep. for *Metrologia*

[22] Massa E, Mana G, Ferroglio L, Kessler E G, Schiel D and Zakel S 2011 The measurement of the ^{28}Si lattice parameter *Metrologia* submitted

[23] Busch I, Azuma Y, Bettin H, Cibik L, Fuchs P, Fujii K, Krumrey M, Kuetgens U, Kuramoto N and Mizushima S 2011 Surface layer determination for the Si spheres of the Avogadro project, in prep. for *Metrologia*

[24] Beckhoff B *et al.* 2009 A quarter-century of metrology using synchrotron radiation by PTB in Berlin *physica status solidi B* **246**, 1415 – 1434

[25] Busch I, Danzebrink H-U, Krumrey M, Borys M and Bettin H 2009 Oxide layer mass determination at the silicon sphere of the Avogadro project *IEEE Trans. Inst. Meas.* **58**, 891 – 896

[26] Seah M P *et al* 2004 Critical review of the current status of thickness measurements for ultrathin SiO_2 on Si - Part V: Results of a CCQM pilot study *Surf. Interface Anal.* **36** 1269-1303

[27] Mizushima S 2004 Determination of the amount of gas adsorption on SiO_2/Si(100) surfaces to realize precise mass measurements *Metrologia* **41** 137-144

[28] Fuchs P 2009 Laboratory report, Bundesamt für Metrologie Bern, Switzerland
[29] Bartl G, Bettin H, Krystek M, Mai T, Nicolaus A and Peter A 2011 Volume determination of the Avogadro spheres of highly enriched ^{28}Si with a spherical Fizeau interferometer, in prep. for *Metrologia*
[30] Kuramoto N and Fujii K 2003 Interferometric determination of the diameter of a silicon sphere using a direct optical frequency tuning system *IEEE Trans. Instrum. Meas*. **52** 631-635
[31] Kuramoto N and Fujii K 2005 Volume determination of a silicon sphere using an improved interferometer with optical frequency tuning *IEEE Trans. Instrum. Meas.* **54** 868-871
[32] Kuramoto N, Fujii K, Azuma Y, Mizushima S and Toyoshima Y 2007 Density determination of silicon spheres using an interferometer with optical frequency tuning *IEEE Trans. Instrum. Meas* **56** 476-480
[33] Kuramoto N and Fujii K 2009 Improvement in the volume determination for Si spheres with an optical interferometer IEEE Trans. *Instrum. Meas* **58** 915-918
[34] Kuramoto N, Fujii K and Yamazawa K 2011 Volume measurement of ^{28}Si spheres by an optical interferometer with a flat étalon to determine the Avogadro constant, in prep. for *Metrologia*
[35] Andreas B, Ferroglio L, Fujii K, Kuramoto N and Mana G 2011 Phase corrections in the optical interferometer for Si sphere volume measurements at the NMIJ, in prep. for *Metrologia*
[36] Kuramoto N, Fujii K, Nicolaus A, Bartl G, Gray M, Manson P and Giardini W 2011 Diameter comparison of a silicon sphere for the international Avogadro coordination project *IEEE Trans. Instum. Meas.* to be published
[37] Picard A, Barat P, Borys M, Firlus M and Mizushima S 2011 State-of-the art mass determination of ^{28}Si spheres for the Avogadro project, in prep. for *Metrologia*
[38] Bettin H and Toth H 2006 Solid density determination by the pressure-of flotation method *Meas. Sci. Technol.* **17** 2567-2573
[39] Waseda A and Fujii K 2004 Density comparison measurements of silicon crystals by a pressure-of-flotation method at NMIJ *Metrologia* **41** S62-S67
[40] Waseda A and Fujii K 2011 Density comparison of isotopically purified silicon single crystals by the pressure-of-flotation method *IEEE Trans. Instum. Meas.* submitted
[41] ISO 1993 *Guide to the Expression of Uncertainty in Measurement* 1st ed. (Geneva: International Organisation for Standardisation) (corrected and reprinted 1995)
[42] GUM Workbench Version 1.2.11.56 ’96-’99 by Metrodata GmbH
[43] Egidi C 1963 Phantasies on a natural unity of mass *Nature* **200** 61-62
[44] Bonse U and Hart M 1965 An X-ray interferometer *Appl. Phys. Lett.* **6** 155-156
[45] Deslattes R D *et al* 1974 Determination of the Avogadro constant *Phys. Rev. Lett.* **33** 463-466
[46] Walker G 2004 A most unbearable weight *Science* **304** 812-813
[47] Rainville S *et al* 2005 A direct test of $E = mc^2$ *Nature* **438** 1096-1097
[48] Steiner R L, Williams E R, Newell D B and Liu R 2005 Towards an electronic kilogram: an improved measurement of the Planck constant and electron mass *Metrologia* **42** 431-441
[49] Steiner R L, Williams E R, Liu R and Newell D B 2007 Uncertainty Improvements of the NIST Electronic Kilogram *IEEE Trans. Instrum. Meas.* **56** 592
[50] Robinson I A and Kibble B P 2007 An initial measurement of Planck´s constant using NPL Mark II watt balance *Metrologia* **44** 427-440, and private communication 2010
[51] Mohr P J, Taylor B N and Newell D B 2008 CODATA recommended values of the fundamental physical constants: 2006 *J. Phys. Chem. Ref. Data* **37** 1187-1284
[52] Gläser M, Borys M, Ratschko D and Schwartz R 2010 Redefinition of the kilogram and the impact on its future dissemination *Metrologia* **47** 419-428